Electrical conductivity in Li2O2 and its role in determining capacity limitations in non-aqueous Li-O2 batteries

Viswanathan, V.; Thygesen, Kristian Sommer; Hummelshøj, J.S.; Nørskov, Jens Kehlet; Girishkumar, G.; McCloskey, B.D.; Luntz, A.C.; Luntz, A.C.

Published in:
Journal of Chemical Physics

Link to article, DOI:
10.1063/1.3663385

Publication date:
2011

Document Version
Publisher's PDF, also known as Version of record

Electrical conductivity in Li2O2 and its role in determining capacity limitations in non-aqueous Li-O2 batteries

V. Viswanathan, K. S. Thygesen, J. S. Hummelshøj, J. K. Nørskov, G. Girishkumar et al.

Citation: J. Chem. Phys. **135**, 214704 (2011); doi: 10.1063/1.3663385
View online: http://dx.doi.org/10.1063/1.3663385
View Table of Contents: http://jcp.aip.org/resource/1/JCPSA6/v135/i21
Published by the American Institute of Physics.

Electrical conductivity in Li_2O_2 and its role in determining capacity limitations in non-aqueous Li-O_2 batteries

V. Viswanathan,[1] K. S. Thygesen,[2] J. S. Hummelshøj,[3] J. K. Nørskov,[1,3] G. Girishkumar,[4] B. D. McCloskey,[4] and A. C. Luntz[3,4,a)]

[1]*Department of Chemical Engineering, Stanford University, Stanford, California 94305-5025, USA*
[2]*Center for Atomic-scale Materials Design (CAMD), Department of Physics, Technical University of Denmark, Fysikvej 1, 28000 Kgs Lyngby, Denmark*
[3]*SUNCAT, SLAC National Accelerator Laboratory, Stanford, California 94025-7015, USA*
[4]*Almaden Research Center, IBM Research, 650 Harry Rd., San Jose, California 95120, USA*

(Received 2 August 2011; accepted 1 November 2011; published online 6 December 2011)

Non-aqueous Li-air or Li-O_2 cells show considerable promise as a very high energy density battery couple. Such cells, however, show sudden death at capacities far below their theoretical capacity and this, among other problems, limits their practicality. In this paper, we show that this sudden death arises from limited charge transport through the growing Li_2O_2 film to the Li_2O_2-electrolyte interface, and this limitation defines a critical film thickness, above which it is not possible to support electrochemistry at the Li_2O_2–electrolyte interface. We report both electrochemical experiments using a reversible internal redox couple and a first principles metal-insulator-metal charge transport model to probe the electrical conductivity through Li_2O_2 films produced during Li-O_2 discharge. Both experiment and theory show a "sudden death" in charge transport when film thickness is ~5 to 10 nm. The theoretical model shows that this occurs when the tunneling current through the film can no longer support the electrochemical current. Thus, engineering charge transport through Li_2O_2 is a serious challenge if Li-O_2 batteries are ever to reach their potential. © *2011 American Institute of Physics*. [doi:10.1063/1.3663385]

I. INTRODUCTION

Over the past couple of years, there has been feverish research activity into non-aqueous Li-air (or Li-O_2) batteries with the hope that a successful Li-air battery could ultimately be developed to give a safe and cost effective secondary battery with ~5 to 10 times the specific energy of current Li-ion batteries. If successfully developed, such a battery would fully enable electric vehicle transportation without range anxiety. In this battery, the net electrochemical reaction is $2Li + O_2 \leftrightarrows Li_2O_2$, with the forward direction describing discharge of the battery and the reverse direction describing charge.[1] The (possible) large increase in specific energy, compared to Li-ion batteries, arises from two sources: (i) one of the reactants, O_2, is not stored in the battery but comes from breathing air as in a fuel cell and (ii) Li metal would be used as the anode rather than Li intercalated graphite (LiC_6) as in Li-ion batteries. However, despite their great promise, many scientific and technical challenges must be overcome if a practical Li-air battery is to ever become a reality.[2]

One of the important challenges for Li-O_2 batteries is the limited capacity (mA h) in discharge relative to that theoretically possible from the pore volume of the cathode. Since the reaction product Li_2O_2 is completely insoluble in the non-aqueous electrolyte, it builds up as a solid in the porous C cathode where it is formed. It has previously been argued[3] that the limited cell capacity is a consequence of electrical passivation of the cathode by the discharge products rather than pore clogging or O_2 transport limitations as claimed by others.[4,5] The suggestion that electrical passivation was a central issue resulted from comparing the discharge capacity of typical Li-O_2 batteries with large surface area porous C cathodes to that observed with low surface area glassy carbon (GC) electrodes, where clogging and O_2 transport issues were negligible. Although the absolute magnitudes of the capacity were different in the two cases, both showed the same qualitative discharge behavior, i.e., a relatively stable discharge potential at ~2.6 V to a certain discharge capacity, followed by a sudden decrease in output potential to <2.0 V (defined as death of the cell). Using an empirically defined electrical resistance through the deposited film as a function of average discharge product thickness fit to the discharge behavior of cells with the GC electrodes, a continuum model (including thermodynamics, transport, and kinetic processes) also described the capacity limitations of Li-O_2 batteries with porous cathodes.[3] In these early experiments, carbonate based electrolytes were used, so that the reaction products were undoubtedly predominately insoluble carbonates rather than Li_2O_2.[3]

In this paper, we investigate electrical conductivity through films of Li_2O_2 both experimentally and theoretically and demonstrate conclusively that electrical conductivity *is* responsible for the capacity limitation of Li-O_2 batteries. In the experiments, we use cyclic voltammetry and impedance measurements of a well known redox couple (ferrocene/ferrocenium) to probe electron (or hole) transport through films of Li_2O_2 grown on flat GC electrodes at various stages of Li-O_2 discharge using dimethoxyethane as the electrolyte solvent (which produces principally Li_2O_2 on

a)Author to whom correspondence should be addressed. Electronic mail: acluntz@pacbell.net.

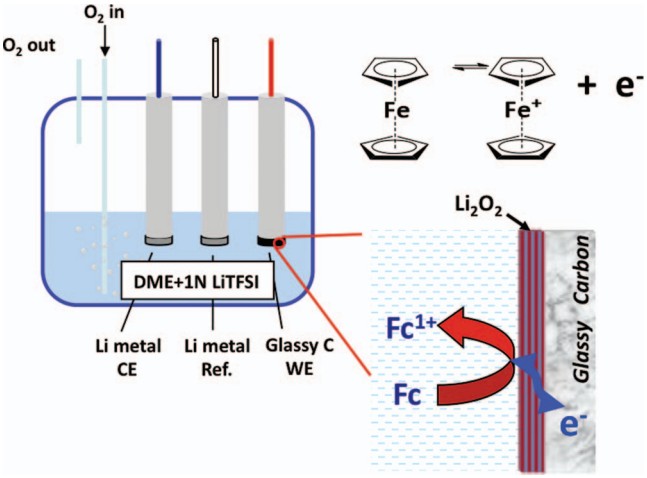

FIG. 1. Schematic diagram of the experiment using the redox couple (ferrocene/ferrocenium) to probe charge transport through films of Li_2O_2 grown on a glassy carbon (GC) working electrode by the electrochemical reaction $2Li + O_2 \rightarrow Li_2O_2$ in a bulk three electrode electrolysis cell.

discharge[6]). These experiments show that the electrical conductivity through the film mirrors the capacity behavior and demonstrates a critical thickness of the Li_2O_2 deposit, above which electron transport to the Li_2O_2–electrolyte surface is inhibited, and hence, electrochemistry cannot be supported. Using a metal-insulator-metal (MIM) representation for the electrochemistry at the cathode of a Li-O_2 cell, first principles transport calculations give a deep understanding of how this critical thickness arises. These calculations show that a mechanism of hole tunneling through the electrically insulating Li_2O_2 film determines the capacity limitations. When the tunneling current is sufficient to drive the electrochemistry, the cell discharge potential U is determined principally by the kinetic overpotential η. However, as discharge progresses and the Li_2O_2 film thickness grows large enough, an exponentially increasing bias across the film is necessary to maintain a tunneling current sufficient to drive the electrochemistry. This bias no longer appears as an output voltage at the cathode. In other words, the cell suddenly fails at a critical Li_2O_2 film thickness.

II. EXPERIMENT

The basic experimental concept is outlined in Fig. 1. A hermetically sealed 3-electrode bulk electrolysis cell containing a 1 M non-aqueous Li salt electrolyte and dissolved O_2 gas allow Li_2O_2 films to be deposited on a smooth glassy carbon cathode during discharge. In addition, the electrolyte contains 3 mM Ferrocene which generates an outer sphere reversible redox couple ferrocene/ferrocenium (Fc/Fc^+) at ~3.4 V relative to Li/Li^+. Since the oxidation/reduction of the Fc/Fc^+ couple only depends upon electron (or hole) transport through the Li_2O_2 film to the solution, the current of this reaction provides a direct measurement of charge transport through the film. This current is followed at various stages of discharge corresponding to different average thickness d of the Li_2O_2 film. It should be pointed out that because the Fc/Fc^+ redox couple is centered at ~3.4 V (Li/Li^+), that some small fraction of the Li_2O_2 film is undoubtedly removed during the oxidation of Fc so that the values of d obtained from the total discharge coulometry may be under estimated.

The bulk electrolysis electrochemical cell has high purity 250 μm thick electrochemical grade Li metal discs as counter and reference electrodes (FMC Corp., Charlotte, NC, USA) and a flat electrochemical grade GC disc for the cathode (Tokai Carbon USA, Hillsboro, OR, USA). All electrodes are ~1.1 cm^2 area. The GC electrode underwent standard cleaning procedures involving polishing with successive grades of alumina paste to a smooth finish followed by sonication in acetone. The electrolyte consisted of ~15 ml of 1 M lithium-bis(trifluoromethanesulfonimide) [LiTFSI] dissolved in dimethoxyethane (DME). The salt and solvent were both high purity electrochemical grade (Novolyte Corp., Cleveland, OH, USA) with <20 ppm H_2O as measured by Karl-Fischer titration. 3 mM high purity ferrocene (Sigma Aldrich, St. Louis, MO, USA) is added to the electrolyte. The air tight cell has both O_2 inlet and outlet ports which allow bubbling of ultrahigh purity O_2 at a pressure of ~1 bar through the electrolyte during discharge to insure that the electrolyte remains saturated with O_2. This also gives considerable stirring action during discharge. The cell and all components are assembled in an Ar glove box (<0.1 ppm H_2O and O_2) and special care is taken to never expose the cell contents to ambient air from beginning to end of the experiments. All electrochemical experiments were performed using a BioLogic VMP3 Multichannel Workstation (Bio-Logic, Knoxville, TN, USA). Previous experiments using high surface area C cathodes have shown that the dominant detectable product formed during discharge is Li_2O_2 with LiTFSI/DME as the electrolyte.[6] XPS and scanning Auger measurements of deposits formed on the GC during discharge are also consistent with this conclusion.

The Li_2O_2 films on the GC are grown using galvanostatic discharge at ~1 $\mu A/cm^2$ current density. Prior to the Li-O_2 cell reaching its end of life (defined as an output voltage U = 2.0 V), the discharge is periodically interrupted every 10–15 min to analyze charge transfer at the Li_2O_2-electrolyte interface. During interruption, the cell is initially open circuited for ~2 min and O_2 bubbling stopped, after which an oxidation and then reduction cyclic voltammetry (CV) of the Fc/Fc^+ couple is performed. Immediately following the reduction cycle while there is a quasi-equilibrium of Fc and Fc^+ at the electrode-solution interface, electrochemical impedance spectroscopy (EIS) is performed to measure the charge transfer resistance of the Fc/Fc^+ redox reaction corresponding to this state of Li–O_2 discharge. The galvanostatic discharge producing Li_2O_2 is then continued for another 10–15 min, followed by interruption to measure the Fc/Fc^+ redox, etc. The procedure is repeated until the cell's end of life. The CV over the Fc/Fc^+ couple are run at a scan rate of 100 mV/s. The EIS is measured using a 10 mV amplitude sine wave applied to the GC/Li_2O_2 electrode under open circuit conditions and scanned over the frequency range of 0.005 Hz to 100 kHz. The charge transfer resistance R_{CT} for the Fc/Fc^+ redox reaction is obtained by measuring the diameter of the charge transfer semicircle along the real axis in a Nyquist plot. The raw impedance data corresponding to the various states

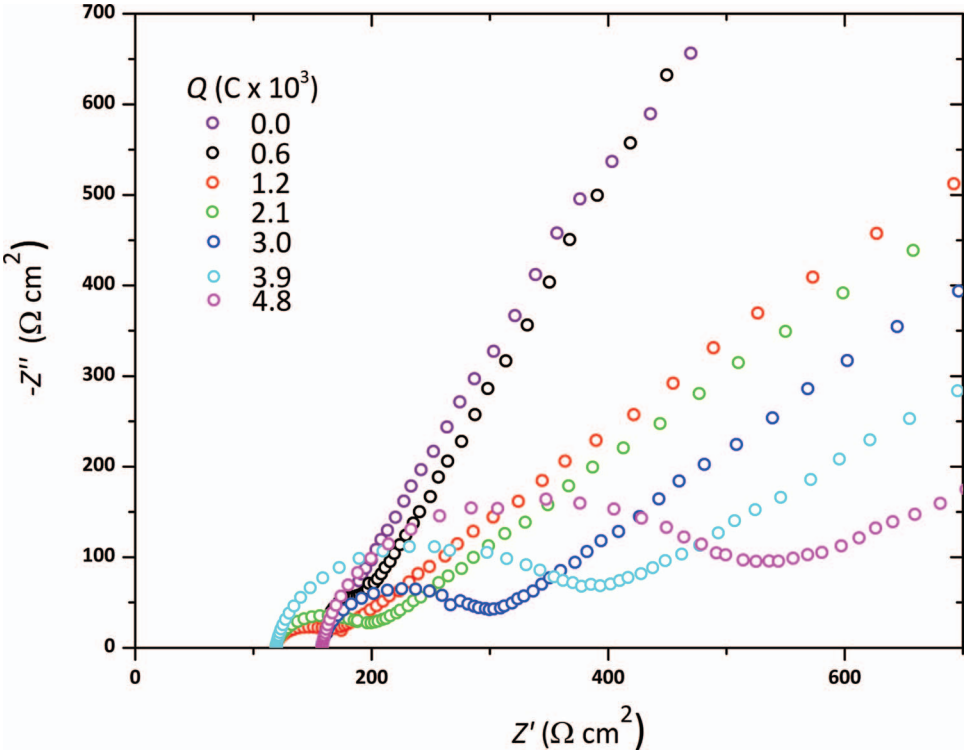

FIG. 2. Nyquist plot (Z″ vs Z′) for the Fc/Fc^+ charge transfer reaction after varying extent of Li-O_2 discharge at ~1 $\mu A/cm^2$ current density. The legend gives the number of Coulombs (C) discharged prior to the impedance spectroscopy. The charge transfer resistance is taken as the diameter of the semicircle along the real axis (Z′).

of discharge are given in Fig. 2. C labels the total number of Coulombs of discharge Q prior to the EIS experiment.

At Q = 0 before the cell is subjected to discharge, a well defined oxidation/reduction peak corresponding to ferrocene redox chemistry is obtained in the CV. However, as the cell is subjected to Li–O_2 discharge, and the CVs are intermittently recorded, several key things happen: (1) The peak separation between Fc $\rightarrow Fc^+$ and $Fc^+ \rightarrow$ Fc redox reactions, ΔE_p, increases, consistent with an increase in R_{CT} (or decrease in exchange current density) and (2) the currents in the redox peaks decreases progressively. After discharging for Q = 0.006 C, the redox peaks disappear completely. Since the current in the Fc/Fc^+ redox CV depends only upon charge transfer, this demonstrates qualitatively that the Li_2O_2 film becomes increasingly electrically insulating as it grows. EIS is used to probe the charge transport quantitatively for various stages of discharge.

Figure 3(a) shows a typical discharge curve, cell output voltage U vs discharge capacity Q (Coulombs), at a current density $j \approx 1$ $\mu A/cm^2$. Also included is the estimated average thickness d of the Li_2O_2 film obtained from Q, the projected area of the electrode, and the bulk density of Li_2O_2 of 2.3 gm/cm^3. This discharge curve shows an immediate drop from the open circuit potential (OCV) to ~2.65 V due to the overpotential for discharge η, then a gently decreasing output potential until the sudden death of the cell, similar to that observed previously in cells with GC electrodes and carbonate based electrolytes.[3] Since employing DME as a solvent has been shown to principally produce Li_2O_2 deposits during discharge, while carbonate solvents produce complex carbonate deposits on discharge,[6] the nature of the capacity limitation is not related to any specific cathode chemistry, but rather only that the deposits be electrically insulating.

Figure 3(a) suggests $d \sim$ 4–5 nm as an average thickness of Li_2O_2 for cell death. Atomic force microscopy measurements of a GC cathode discharged under similar conditions gives an average thickness of $d = 7 \pm 3$ nm at cell death and 3 ± 2 at half the Q required for cell death. These experiments used multiple contact mode scans with a boron doped diamond tip to erode the electrochemical deposit from a given area until a constant conductivity was obtained from the GC substrate (which does not erode under these forces). Tapping mode scans of the topology through the eroded and non-eroded regions give the average d of the electrochemical deposits. These experiments show that the electrochemical deposits fully covered the GC surface, albeit with a rms roughness of ~3 to 4 nm above that of the GC film. These experiments will be reported in detail elsewhere.[7]

In a separate experiment, the cell was also discharged with the added ferrocene in the manner described above. Discharging at constant current density to electrodeposit Li_2O_2 by passing known charge Q and simultaneously following the electrochemistry of Fc/Fc^+ allows us to probe charge transport at various points on the discharge curve. Figure 3(b) shows the exchange current density j_0 for the Fc/Fc^+ redox reaction as a function of Q and d. j_0 is obtained from the charge transfer resistance R_{CT} from the analysis of the EIS according to $j_0 = R_g T/FR_{CT}$, where R_g is the universal gas constant, T is the absolute temperature in degrees Kelvin, and F is the Faraday's constant. The impedance scans from which

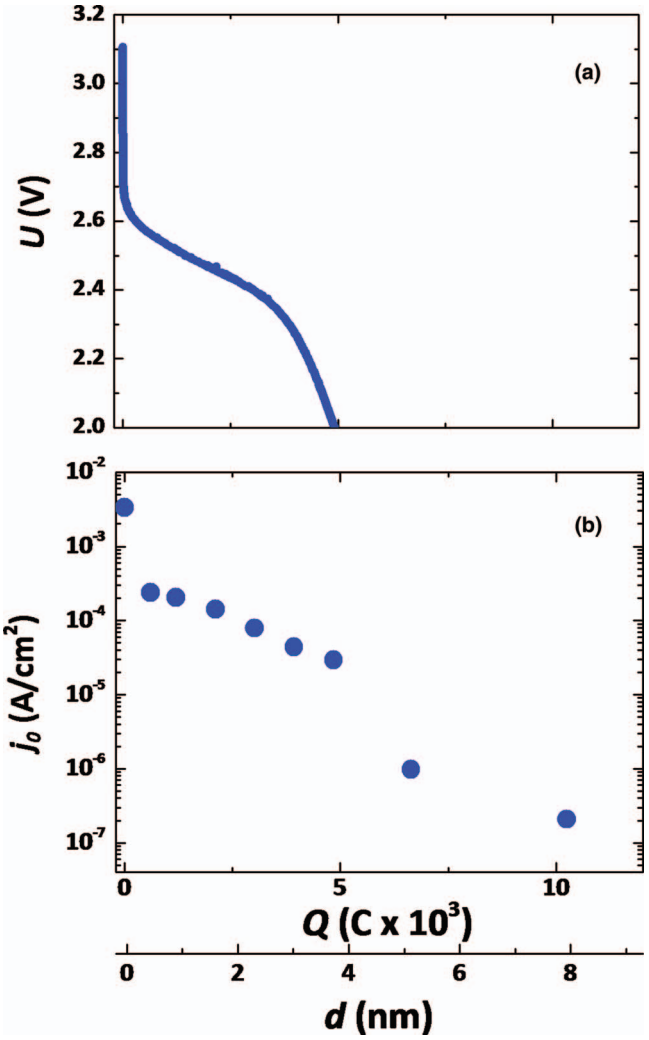

FIG. 3. (a) Discharge capacity of a Li-O_2 cell at ~1 μA/cm^2 discharge current density, plotted as cell potential U vs extent of discharge Q (Coulombs) and average thickness d of the Li_2O_2 film grown on the glassy carbon substrate. (b) Exchange current density j_0 for the charge transfer reaction Fc/Fc$^+$ obtained from impedance spectroscopy as a function of Q and d for Li-O_2 discharge under similar conditions as in (a).

R_{CT} is obtained are shown in Fig. 2. j_0 shows an immediate drop of approximately an order of magnitude with very minimal discharge, presumably due to scattering of charge carriers at the interface or partial passivation of electrochemically hyperactive defect sites. This is followed by a more gradual decrease in j_0 until a thickness of ~5 nm, after which j_0 falls rapidly to values of ~10^{-7} A/cm^2 at larger d. At large d, the impedance is almost exclusively capacitive so that it is difficult to extract meaningful values of R_{CT}. Thus, the value at 8 nm should only be considered as an upper bound to j_0. The sharp decrease in j_0 at $d \sim 5$ nm defines a critical thickness of Li_2O_2 above which it no longer supports electrochemistry at its electrolyte interface. Since j_0 depends only upon electrical conductivity through the film, this critical thickness arises solely from charge transport issues. In addition, since the capacity behavior in the Li-O_2 cell is so similar to that of j_0 for the Fc/Fc$^+$ redox couple, this demonstrates that sudden cell death arises from the existence of the critical film thickness for electrical conductivity.

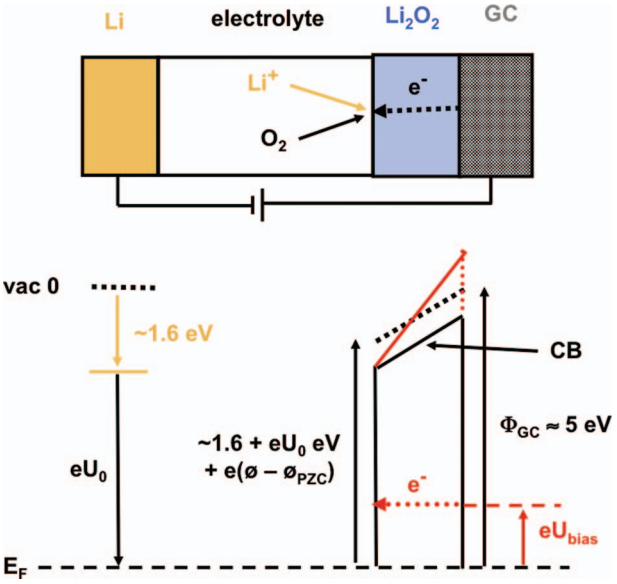

FIG. 4. Schematic of a typical Li-O_2 cell during discharge. GC refers to the cathode. The arrows labeled Li^+, O_2, and e^- show the path of the three reactants in the cell. In the lower part of the figure is a schematic of the electron energies in the various regions of the cell, all referenced to vacuum zero. Note that there is a significant barrier to charge transport shown here as the difference between the conduction band (CB) and the Fermi energy E_F. The red part shows what happens when a bias is applied to the equilibrium state of the cell.

Figure 4 shows a schematic of a typical Li-O_2 electrochemical cell during discharge. This schematically indicates the path of the three reactive components necessary for electrochemistry: Li^+, O_2, and e^-. Figure 4 schematically indicates the electron energies within the different elements of the cell. At the equilibrium potential U_0 of a redox couple, e.g., Fc/Fc$^+$ or Li-O_2, the Fermi energy E_F is constant throughout the cell. The energy of vacuum zero, E_0, is indicated by the dotted lines. The energy for Li relative to vacuum zero (1.6 V) is taken from the potential of the standard hydrogen electrode (4.5 V) and the Li/Li$^+$ potential relative to the standard hydrogen electrode in the non-aqueous solvent (2.9 V). Neglecting any Schottky barriers, E_0–E_F at the GC-Li_2O_2 interface is given by the work function of GC, ~5 eV. At the electrolyte-Li_2O_2 interface, $E_0 - E_F = 1.6 + eU_0 + e(ø - ø_{PZC})$, where the first term is the energy of Li/Li$^+$ relative to vacuum zero, the second term is the energy of the redox couple relative to Li/Li$^+$, and the third term accounts for any charging at the Li_2O_2-electrolyte interface, i.e., deviation of the interface from the potential of zero charge. Since Li_2O_2 is a wide bandgap insulator, it is likely that the conduction band (CB) is several eV above E_F. Upon application of a bias eU_{bias} (shown in red) across the Li_2O_2 film, electrons only reach the electrochemical interface via transport through the previously grown peroxide layer. Thus, this electron transport is essentially equivalent to that observed in a biased metal insulator metal (MIM) junction. Note that Fig. 4 is drawn assuming some charging at the Li_2O_2–electrolyte interface.

In the following, we develop a first principles theoretical MIM model and show how charge transport through Li_2O_2 defines the critical thickness observed in the experiments. Note that in the absence of substantial charging at

the electrolyte-Li_2O_2 interface, the potential barrier is nearly symmetrical so that we use a symmetrical MIM model to describe the conductivity. We also note that when hole conductivity is dominant (as we show later to be the case for Li_2O_2), an equivalent picture for hole energies simply involves interchanging the conduction band by the valence band of Li_2O_2.

III. THEORY

Galvanostatic discharge in the Li-O_2 battery depends on many interrelated factors, e.g., the thermodynamics and kinetics of the charge transfer processes, the surface composition, the transport of all species to the electrochemically active interface, and the nucleation and growth of the Li_2O_2 product. In this section, we develop a model for the charge transport through previously deposited Li_2O_2 films since this limits capacity during discharge. However, we will show later that this charge transport depends upon the surface species present during discharge and this, in turn, depends upon the thermodynamics and kinetics of the electrochemistry and the growth mechanism, so that we first briefly discuss these aspects of the discharge. Since the electrochemistry ultimately also depends on the charge transport, we develop a self-consistent model to couple the electrochemistry and the conductivity to explain the origin of the capacity fall-off observed in the Li-O_2 batteries.

A. Growth mechanism of Li_2O_2

We assume that after an initial nucleation phase of Li_2O_2 on GC, that the electrochemistry is dominated by Li_2O_2 formation on Li_2O_2, that is, Li_2O_2 crystal growth. This assumption is certainly valid for deep discharges corresponding to death of the cell and there is ample experimental evidence for complete film formation on flat GC electrodes.[2,3] In addition, the AFM measurements mentioned above clearly show that the GC surface is fully covered with the electrochemical deposit, both prior to and at sudden cell death. In fact, it is hard to rationalize the electrical passivation of the smooth GC cathode without the electrochemical deposit fully covering the electrochemically active GC surface. Since the AFM measurements suggest some variations in the thickness of the electrochemical deposit, the actual nucleation-growth of Li_2O_2 on itself must be somewhat complicated. However, for simplicity in the charge transport calculation we simply assume a layer by layer growth process, i.e., that we are dealing with a fixed d corresponding to a number of layers rather than some average d for a range of thicknesses. It is generally assumed that crystal growth occurs principally at kink and step sites since these allow the most stabilization of adspecies.[8] This, of course, implies that intermediates are somewhat mobile on the Li_2O_2 surface. Since Li-O_2 discharges form Li_2O_2 crystallites of ~15 nm dimensions (from x-ray analysis),[6] we take this mechanism to be dominant in the growth during discharge. In particular, the thermodynamics for Li_2O_2 electrochemistry on Li_2O_2 steps has been discussed previously[8] so that we use this mechanism to investigate charge transport during electrochemistry. This mechanism is given in terms of the following steps of charge transfer:

$$(1)\ \mathrm{Li} \rightleftarrows \mathrm{Li^+} + \mathrm{e^-} \quad \text{(anode)},$$

$$(2)\ \mathrm{Li^+} + \mathrm{e^-} + \mathrm{O_2^*} \rightleftarrows \mathrm{LiO_2^*} \quad \text{(cathode)},$$

$$(3)\ \mathrm{Li^+} + \mathrm{e^-} + \mathrm{LiO_2^*} \rightleftarrows \mathrm{Li_2O_2^*} \quad \text{(cathode)},$$

where the * refers to surface adsorbed species on the step sites.

B. Thermodynamics at steps

Since the most stable Li_2O_2 surface, reconstructed $Li_2O_2(1\bar{1}00)$ (previously labeled 100 in Ref. 7), contains two formula units of Li_2O_2 in a unit cell, reaction steps (1)–(3) above need to run twice before the initial and final states of the surface are the same. Figure 5 shows the calculated free energy diagram at four different potentials U for reactants, products, and the intermediates in the reaction. The potential dependence is given by $-neU$, where n is the number of $Li^+ + e^-$ for each step. The standard potential is $U_0 = 2.71$ V and is closer to the experimental one of 2.96 V than that reported earlier[8] due to a better description of the Li bulk energy (using the RPBE functional used in the rest of the calculations). The theoretical overpotential (η) is defined as the potential at which all steps are thermodynamically downhill relative to U_0, i.e., for discharge $\eta_{dis} = 2.71$ V – 2.26 V = 0.45 V and for charge $\eta_{chg} = 3.32$ V – 2.71 V = 0.61 V. We have found, quite generally, that this theoretical overpotential describes quite well the onset potential at which ion transfer surface electrochemical reactions have an appreciable rate.[9–11] This implies that activation barriers in the individual steps in the kinetic mechanism are not determining the overpotentials. At the equilibrium potential, a mixed phase of LiO_2^*, its dimer $2LiO_2^*$, and Li_2O_2 coexist at the surface. The potential limiting step during discharge (η_{dis}) is the addition of Li^+ to a LiO_2^*, while the generation of $O_2^* + Li^+ + e^-$ from $2LiO_2^*$ is potential limiting in charge (η_{chg}).

C. Kinetic model

Since the surface concentration of species changes with applied potential**,** we use a simple kinetic model to calculate the potential-dependent coverage of different species along the steps during discharge and charge. The rates of each of the electrochemical steps in Fig. 5 are represented by simple Butler-Volmer expressions with rate constants given by $k_i = k_i^0 \max[\exp\{-\alpha\,(eU - \Delta G)/k_B T\},\ 1]$, with k_i^0 the pre-exponential and the exponential term describing the potential dependent energy terms. The max notation guarantees that when $\Delta G \gg eU$ that $k_i = k_i^0$. In this model, we set $\alpha = 1$ so that only thermodynamic limitations are included in the kinetics.[12] There are undoubtedly additional kinetic barriers associated with the de-solvation of Li^+ in each of the steps, but this is included in the pre-factors k_i^0 since these are likely to be nearly the same for each of the steps, and hence, principally affect the absolute magnitudes of the rates rather than the a potential dependence in the relative kinetics between

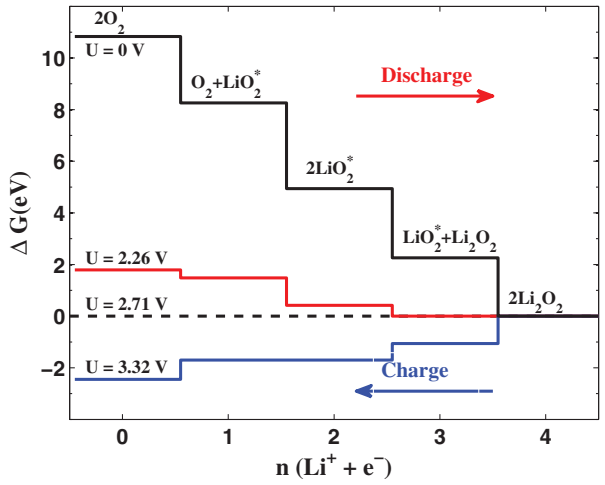

FIG. 5. Calculated free energy diagram for the reactions at the oxygen electrode of a Li-air battery. Two formula units of Li_2O_2 are added during discharge (left to right) or removed during charge (right to left). The free energies are shown at different potentials; $U = 0$, $U = 2.71$ V is the open circuit potential, $U = 2.26$ V is the highest potential where discharge is still downhill in all steps, and $U = 3.32$ V is the lowest potential where charging is all downhill.

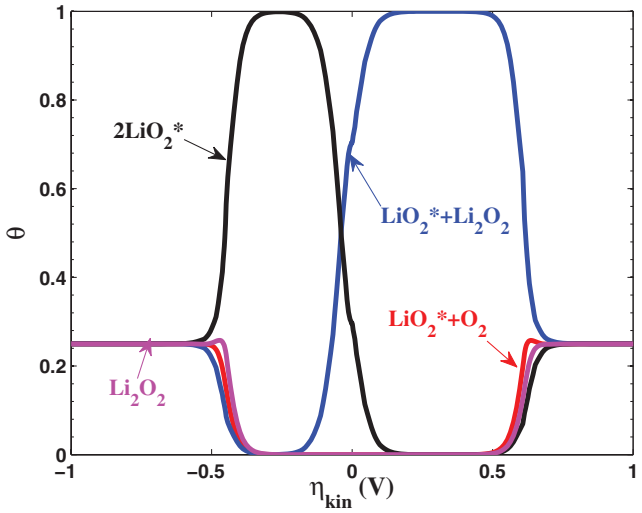

FIG. 6. The relative surface population of different species in the free energy diagram as a function of the overpotential during discharge (negative) and charging (positive). The species marked as $2LiO_2$ is the vacancy dimer.

steps. In fact, k_i^0 is assumed the same for each of the steps in the kinetics. Since the Li_2O_2 surface considered in Fig. 5 contains two formula units per unit cell, we model the kinetics using a two site model for the different LiO_2^* intermediates. This simple two-site model distinguishes between the two different LiO_2^* containing species involved in the basic growth process. When the LiO_2^* is occupied on both of these sites, we refer to this state as the vacancy dimer labeled $2LiO_2^*$. The coupled kinetic equations are solved for the relative step coverage of the different species as a function of U using a transient model akin to a linear sweep voltammetry experiment. The results using the transient model are nearly identical to those obtained with an equivalent steady-state model of the coupled kinetics. The relative coverage of the various species as a function of U is given in Fig. 6. At the discharge overpotential $\eta = 0.45$ V, there is a significant sensitivity of the species coverage with U. As will be seen later, the magnitude of the charge transport depends on the concentration of LiO_2^* (or $2LiO_2^*$) at the surface, so the θ_i of Fig. 6 are necessary to determine the transport at a given U.

D. Charge transport

Because charge transport through the electrochemical deposit during cell discharge resembles that of a MIM, we utilize a theoretical MIM configuration consisting of Au|Li_2O_2|Au layers to investigate the charge transport through Li_2O_2 films. Since metal electrodes are chosen to mimic both the electrolyte and the GC cathode, the calculations probes the pure charge transport of the Li_2O_2 films. Nevertheless, the work function of Au is quite similar to that of GC. Using Au in place of the electrochemical discharge reaction is equivalent to using a perfectly reversible redox couple in the electrochemistry. Therefore, the current calculated through the MIM structure depends only on the conductivity of the peroxide film.

All transport calculations are performed within density functional theory[13,14] as implemented in the GPAW package[15,16] using the Atomic Simulation Environment.[17] The GPAW package is a real space grid algorithm based on the projector augmented wave function method with a frozen core approximation. The finite bias transport calculations are performed using a non-equilibrium Green's function (NEGF) method as implemented within GPAW.[16] Following the standard notation used in the electron transport literature, we refer to the Li_2O_2 slab and four layers of Au on each side as the central region (C) and bulk metallic Au as left (L) and right (R) leads. The left (L) and right (R) leads are kept at different chemical potentials μ to simulate an applied bias voltage of $U_{\text{bias}} = (\mu_L - \mu_R)/e$ across the central region. As a consequence of electronic screening, the potential inside the electrodes converges rapidly to the bulk value and sets the boundary conditions for the electrostatic potential inside C. Rather than obtaining the wave functions from the eigenvalue equation, the transmission is solved by using the NEGF of the central region and more details about this method can be found elsewhere.[18] The electron transport calculations are performed using a localized LCAO basis set, i.e., linear combination of atomic orbitals, as implemented in GPAW.[19]

Because the electrolyte facing surface concentrations of the LiO_2^* and Li_2O_2 species vary with U during discharge, we investigate electronic transport through Li_2O_2 films for the two limiting cases given in Fig. 7, i.e., with Li_2O_2 at both the surfaces and for LiO_2^* at one of the surfaces. Reconstructed Au(110) was chosen for the MIM electrode surface as it has the closest registry with the Li_2O_2 structure and charge transport through the interface depends slightly on this. The energy of the structure of the Li_2O_2 used to match the Au(110) surface is within 0.02 eV/formula unit of the bulk structure and corresponded to ~5% mismatch in lattice constants The interfaces were then structurally relaxed using a 4 layer Au

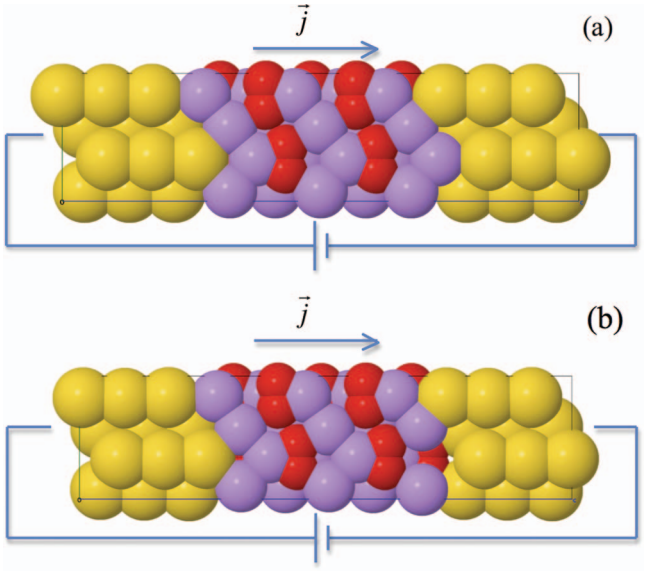

FIG. 7. Typical conductivity calculation setup for (a) Au(110)|Li_2O_2|Au(110) and (b) Au(110)|Li_2O_2-LiO_2|Au(110).

slab and 5 layers of Li_2O_2/Li_2O_2+LiO_2 in the direction normal to the interface. This structural relaxation was minimal. In any event, the exact structure of the interface only weakly affected the magnitude of the conductivity. The distances from the relaxed slab was used to construct a bulk system of alternating layers of Au (5 layers) and Li_2O_2 (5 layers). The central monolayer of Au and Li_2O_2 were fixed and the remaining atoms were relaxed. Subsequent structures for thicker layers were built up by adding layers of Li_2O_2 to the center using its bulk geometry when this had been matched to the lattice of Au and relaxed in the transport direction. Sensitivity to the choice of the electrode material was checked by using Pt(110) as the electrode interface for the pure Li_2O_2 films. The transport results were qualitatively similar to that for Au(110) electrodes and the Li_2O_2 film since they depend principally on the electronic properties of the Li_2O_2 (and the tails of the metal *s*,*p* wave functions that is similar for the two metals). It is likely that there would be larger differences in the transport calculations for the two metals in the Li_2O_2-LiO_2 structures due to the higher reactivity of Pt(110).

The geometric relaxation and energies of the stable interface structures were calculated with GPAW in its normal real space mode with a grid spacing of h = 0.18, which is sufficient for high energy accuracy. These relaxed structures were then used for the electron transport calculations using an LCAO basis set. While the energetics obtained from a limited LCAO basis set is not very accurate, it is suitable for the transport calculations. For the transport calculations, the central region describing the metal-(Li_2O_2/Li_2O_2+LiO_2)-metal interfaces contains 4 layers of metal on either side and varying layers of Li_2O_2/Li_2O_2+LiO_2 between the metal. We have verified that this is sufficient to achieve convergence of the current and potential drop across the interfaces. The electrode regions, i.e., Au(110), were calculated with normal density functional theory (DFT) with periodic boundary conditions. We used a (6,2,1) k-point sampling for the NEGF self-consistent loop and a (12,4,1) k-point grid for evaluating the

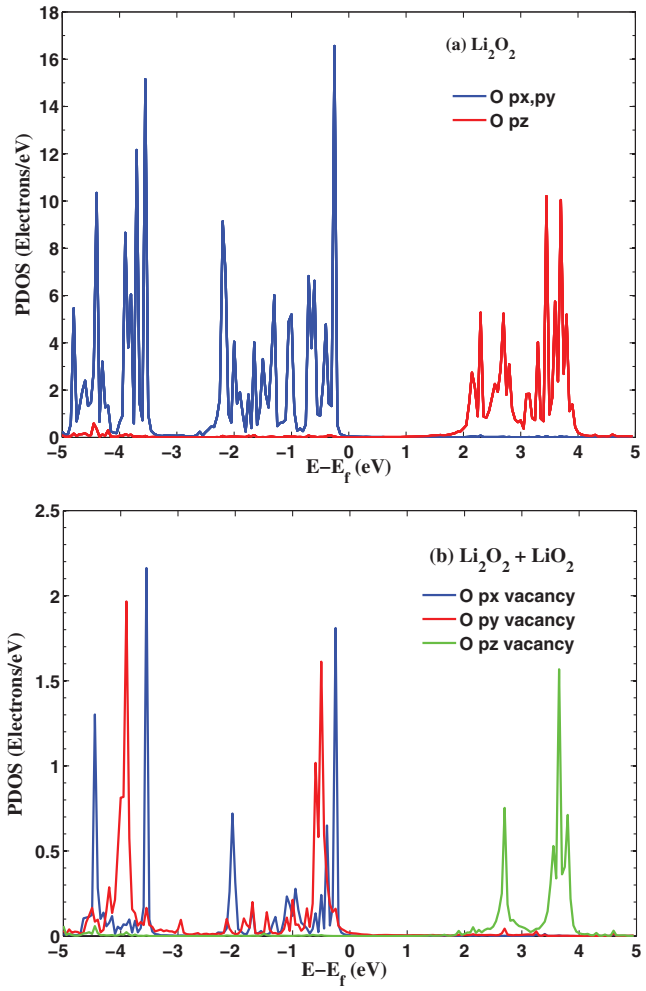

FIG. 8. The PDOS relative to the Fermi energy for (a) the O atoms of the Li_2O_2 system and (b) the O atoms in the LiO_2 layer of Li_2O_2-LiO_2 system.

current. The PBE functional is used for exchange-correlation, and a LCAO basis set corresponding to single-zeta plus polarization is adopted for all atomic species. We have verified that the transport results are converged with respect to the size of the minimal LCAO basis set by comparing some transport calculations to those using a double-zeta plus polarization basis. In the finite bias calculations, a positive bias is defined as passing current from the left to the right, i.e., passing current from the metal to Li_2O_2, corresponding to battery discharge and negative bias corresponds to battery charge.

Figure 8(a) shows the projected density of states for the O p_x, p_y, and p_z orbitals of Li_2O_2 at $U = 0$ when sandwiched between the Au(110) electrodes. The p_x, p_y orbitals are the dominant contributions to the valence band and p_z orbital is the dominant contribution to the conduction band of Li_2O_2.[20] Note that in this calculation the location of these bands relative to the Fermi energy E_F is well defined because of the Au(110) electrodes. The bandgap of Li_2O_2 is poorly described in DFT and GW calculations show that this is almost exclusively due to an artificial lowering of the conduction band by ~3 eV in DFT.[8,20] At both levels of description, the Fermi level is close to the valence band and electrical conductivity is therefore dominated by holes rather than electrons. Since the valence band is well described by DFT, we

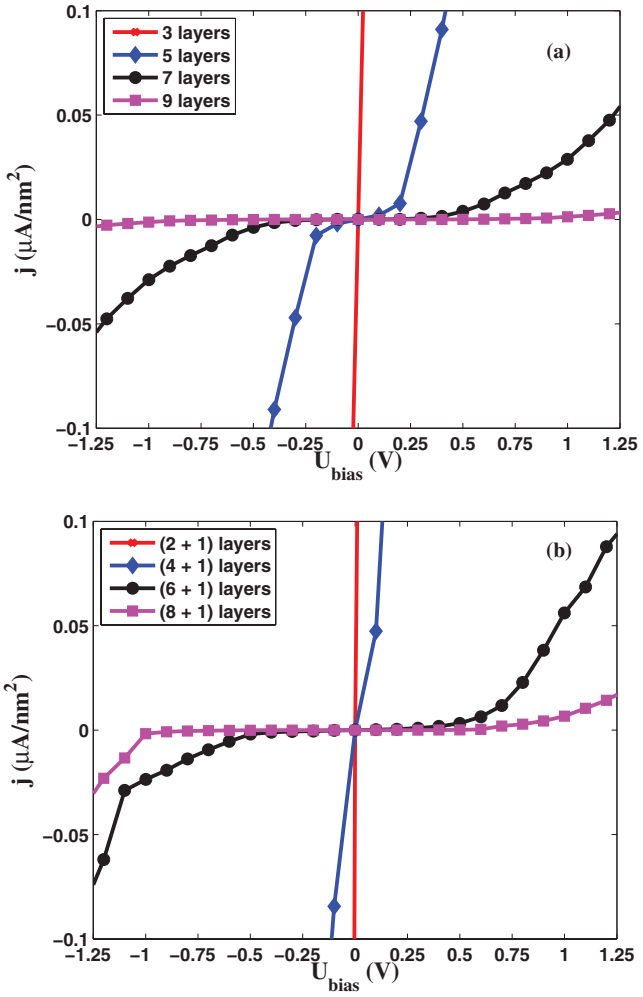

FIG. 9. Calculated current-bias curves for the two different calculation setups as a function of number of layers between the electrodes of (a) pure Li_2O_2 and (b) Li_2O_2 + 1 layer LiO_2 at the interface.

use that level of description in the calculation of conductivity. The O p_x, p_y, and p_z orbitals for the LiO_2 layer of the Li_2O_2-LiO_2 structure are shown in Fig. 8(b). It can be seen that the Fermi level is pinned by the O $2p_y$ orbital of the vacancy layer of LiO_2.

Figure 9 shows the calculated current-bias response curve for the Li_2O_2 and Li_2O_2-LiO_2 structures of varying thickness (number of layers of Li_2O_2). In Fig. 9, the current for a fixed thickness exhibits the roughly linear + exponential dependence with bias characteristic of MIM structures.[21] The current in Fig. 9(a) is symmetric with the sign of bias due to the symmetric nature of the interfaces. On the other hand, Li_2O_2-LiO_2 structures in Fig. 9(b) have a slight asymmetry due to the asymmetry of the interfaces.

Figure 10 shows the current at different fixed bias (±0.1 and ±0.6 V) as a function of the film thickness d, defined as the distance between the innermost Au layers in the two electrodes for the given number of Li_2O_2 layers in the central region. A bias of + 0.1 V is characteristic of the onset of the exponential decrease in cell voltage, while a bias of + 0.6 V is characteristic of complete cell death. The current decays exponentially with d for a fixed bias, with a steeper decay for the lower bias potentials. At fixed bias and d, the current is always higher when LiO_2 is present at the interface. This is completely as anticipated from the projected density of states (PDOS) since LiO_2 p_y states are pinned at E_F, and we thus get better conductivity when the surface species is LiO_2^*. This is the major reason that it is important to know the actual surface composition during discharge in order to compare with experiment.

IV. THEORY—EXPERIMENT COMPARISON

In this section, we use a simple model combining the electrochemistry and transport limitations to construct a theoretical capacity plot to compare with that observed

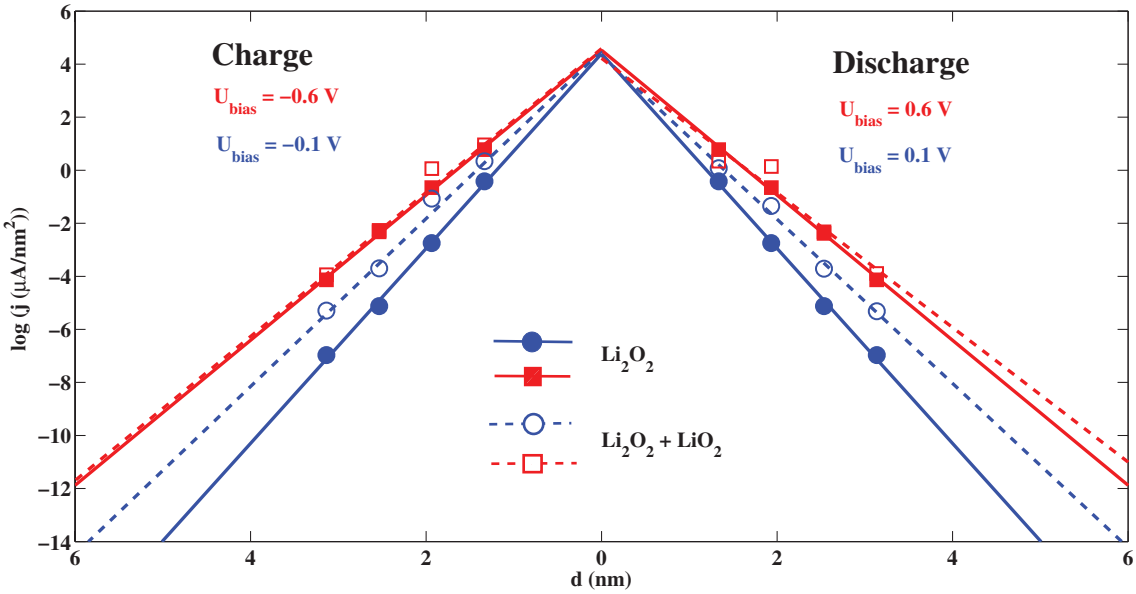

FIG. 10. Conductance plot at two fixed biases as a function of the distance between the electrodes as defined by the number of layers. Solid points are for Li_2O_2 while open points are for Li_2O_2 with LiO_2 at the surface of one electrode.

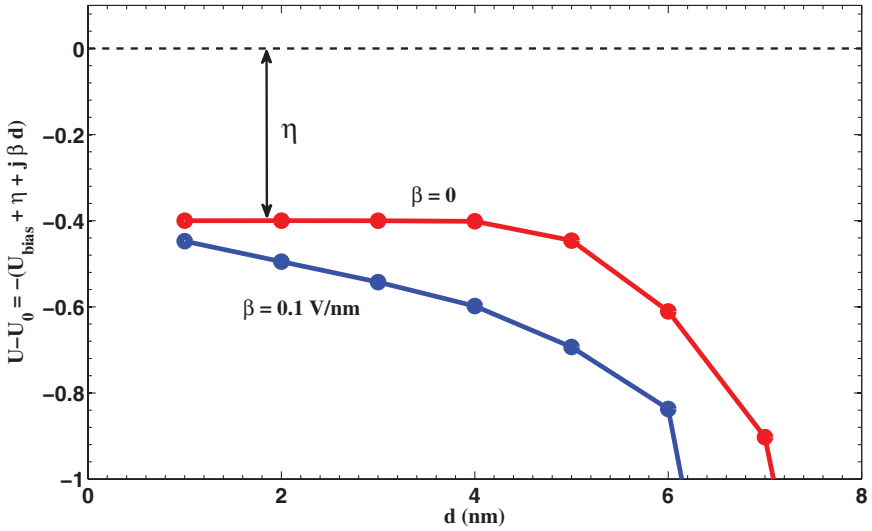

FIG. 11. A theoretical capacity plot of the cell voltage as a function of the length of the Li_2O_2 interlayer spacing (with the appropriate species surface concentrations θ determined by the electrochemistry at the given potential surface potential U-η for a discharge current density $j = 1\ \mu A/cm^2$. At this discharge condition, $\theta(LiO_2^*) \approx 0.9$ and $\theta(Li_2O_2^*) \approx 0.1$.

experimentally [see Figure 3(a)]. The current density can be written as the electrochemical reaction rate (or current j) subject to the conditional constraint that the rate of charge transport through the Li_2O_2 film j_t is sufficient to drive the required electrochemical current. This can be written as

$$j = j_0 \exp(-\{\Delta G(\eta) - \Delta G(\eta = 0)\}/R_g T) \big| [j_t(\theta, U_{bias}) \geq j],$$

where j_0 represents the exchange current density, η is the overpotential, $\Delta G(\eta) - \Delta G(\eta = 0)$ is the free energy shift of the rate limiting step at $U - U_0$, and j_t is the rate or current for charge transport from one Au(110) interface through the film to the other interface which depends on both the bias U_{bias} and the population of the surface species θ. U_{bias} is the potential drop across the film. The surface species θ for j_t is taken as the appropriate linear combination of j_t through pure Li_2O_2 and Li_2O_2-LiO_2 as defined by $U - U_{bias}$. In terms of an equivalent electrical circuit for galvanostatic discharge at dc (where capacitances can be ignored), this rate expression can be rewritten as current at an applied potential U through two resistances that are in series and additive; one representing the film resistance R_{film} (which depends on bias and surface composition) and the charge transfer resistance for the electrochemical reaction R_{CT} which depends upon kinetic overpotential. At a fixed length d, the following equation represents the overall resistance:

$$R_{tot}(U, \theta) = R_{film}(U_{bias}, \theta) + R_{CT}(\eta) \quad \text{with}$$
$$U = U_0 - U_{bias} - \eta,$$

R_{film} depends on the population of the different species θ, which is itself an implicit function of $U - U_{bias}$. U_{bias} is determined by the bias needed to give the required electrochemical current across the film. This is dependent on the thickness of the film grown and the population of the surface species. As a result, the problem needs to be solved in a self-consistent way, where a guess for the state of the surface species is obtained by using the thermodynamic overpotential obtained for the growth process. Using that guess for the population of different species, the film resistance is calculated. Using the potential at the electrolyte interface, we once again solve for the surface species and continue until convergence is obtained. This is repeated as d increases. The calculation of the film resistance for larger lengths is done using an exponential fit to the calculated data at fixed bias, as shown in Fig. 10.

Figure 11 shows the calculated capacity plot for galvanostatic discharge at a current density of $j = 1\ \mu A/cm^2$ and $\eta = 0.45$ V. For $d < 5$ nm, there are no electrical conductivity limitations so that the galvanostatic discharge potential is determined solely by the kinetic overpotential for charge transfer, η. For $d > 5$ nm, conductivity limitations dominate and the cell voltage drops off exponentially with d. The exponential drop in U at $d \sim 5$ nm is the fundamental origin of the phenomenon described as a critical thickness for supporting electrochemistry that is observed in the experiments.

In this model of a perfect crystalline Li_2O_2 lattice and without considering phonons, there is no mechanism for resistivity in the film. Electrical conductivity occurs solely through tunneling of holes through the barrier defined by the valence band and E_F. In reality, Fig. 3 indicates that there is resistivity in the film prior to reaching the critical thickness because of the gradual drop in U in Fig. 3(a) or in j_0 in Fig. 3(b). This is likely due to defects produced in the film during growth. Therefore, we also consider a case where a phenomenological resistance that is proportional to d is added to the equivalent circuit to account for defect scattering. This gives the following expression for R_{tot}:

$$R_{tot}(U, \theta) = R_{film}(U_{bias}, \theta) + R_{CT}(\eta) + \beta d \quad \text{with}$$
$$U = U_0 - U_{bias} - \eta - j\beta d,$$

where β is chosen to give a voltage drop of ~0.1 V/nm as observed in the experiments. In this case, the voltage drop across the interface increases as the film grows and this results in a shift of the most stable surface species from LiO_2^* to $Li_2O_2^*$

as the film grows. This leads to some effect in the fall-off length as $Li_2O_2^*$ is less conducting compared to LiO_2^* surface species (see Fig. 10). The results obtained from this model are in good agreement with the experiments. This highlights the strong coupling that the electrochemistry and conductivity play in determining the discharge characteristics of the Li-air battery.

V. SUMMARY AND CONCLUSIONS

In this paper, we use both electrochemical experiments and first principles theory to probe and understand the origin of the phenomenon of sudden death in Li-O_2 cells which limit their capacity to far less than the theoretical maximum. We show that the sudden death is related to a critical thickness of Li_2O_2 deposit, above which charge transport to the Li_2O_2-electrolyte interface is insufficient to support the electrochemistry.

The experiments use a reversible outer sphere redox couple (ferrocene/ferrocenium or Fc/Fc^+) to probe charge transport through films of Li_2O_2 electrochemically grown on a smooth glassy carbon electrode by Li-O_2 discharge. Both cyclic voltammetry and electrochemical impedance spectroscopy of the redox couple as a function of discharge capacity (or film thickness) show that even this reversible redox reaction shows a sudden death at film thickness nearly identical to that of the Li-O_2 cells. Since the Fc/Fc^+ redox only depends upon charge transport to the Li_2O_2-electrolyte interface, we conclude that these charge transport limitations are also responsible for the sudden death in the Li-O_2 cells.

A first principles MIM model using Au(110) electrodes is developed to probe electrical conductivity through Li_2O_2 films of varying thicknesses. Bias dependent charge transport is calculated using the non-equilibrium Green's function method as implemented in GPAW. Since the electrical conductivity depends on the species present at the Li_2O_2-electrolyte interface (LiO_2, $2LiO_2$, and Li_2O_2) as well as the potential bias across the film, and the species present at the interface depends on the potential and charge transport to the interface, a self-consistent model is developed to treat the charge transport and electrochemistry simultaneously. The calculations show that charge transport is dominated by tunneling of holes and this gives a natural explanation for a critical thickness to support electrochemistry. When the film thickness is less than the critical thickness, the tunneling current is sufficient to support the electrochemistry. However, when the film thickness is greater than the critical thickness, the output potential dies exponentially as the bias required to support the electrochemical current increases exponentially. The critical thickness calculated from the MIM model is in very good agreement with that observed experimentally in actual cells and the redox couple experiments.

Charge transport calculations for the (reconstructed) $Li_2O_2(0001)$ surface using Au(111) electrodes showed a very similar exponential decrease in conductivity with d and with magnitudes similar to that reported here. Therefore, the phenomenon of sudden death in cell discharge at a Li_2O_2 film thickness of 5–10 nm is anticipated to be independent of the growth direction. A detailed comparison of charge transport in the two directions will be reported later.

We believe that the conductivity limitations discussed here are a significant challenge for developing practical Li-air batteries. Engineering higher charge transport through doping or some other strategy will undoubtedly be necessary if one is ever to realize the promise of a high specific energy Li-air battery.

ACKNOWLEDGMENTS

We wish to thank Tom Jaramillo for originally suggesting the use of a redox couple to experimentally probe charge transport through Li_2O_2 films and Jingzhe Chen for helpful discussions on the transport calculations. Support from the Department of Energy, Basic Energy Sciences through the SUNCAT Center for Interface Science and Catalysis and from the Lundbeck Foundation through the Center for Atomic-scale Materials Design is gratefully acknowledged.

[1] K. Abraham and Z. Jiang, J. Electrochem. Soc. **143**, 1 (1996).
[2] G. Girishkumar, B. Mccloskey, A. C. Luntz, S. Swanson, and W. Wilcke, J. Phys. Chem. Lett. **1**, 2193 (2010).
[3] P. Albertus, G. Girishkumar, B. McCloskey, R. S. Sánchez-Carrera, B. Kozinsky, J. Christensen, and A. C. Luntz, J. Electrochem. Soc. **158**, A343 (2011).
[4] J. Read, K. Mutolo, M. Ervin, W. Behl, J. Wolfenstine, A. Driedger, and D. Foster, J. Electrochem. Soc. **150**, A1351 (2003).
[5] S. Sandhu, J. Fellner, and G. Brutchen, J. Power Sources **164**, 365 (2007).
[6] B. McCloskey, D. Bethune, R. Shelby, G. Girishkumar, and A. Luntz, J. Phys. Chem. Lett. **2**, 1161 (2011).
[7] K. Virwani, R. Shelby, and A. Speidel (unpublished).
[8] J. S. Hummelshøj, J. Blomqvist, S. Datta, T. Vegge, J. Rossmeisl, K. S. Thygesen, A. C. Luntz, K. W. Jacobsen, and J. K. Nørskov, J. Chem. Phys. **132**, 071101 (2010).
[9] J. Nørskov, J. Rossmeisl, A. Logadottir, L. Lindqvist, J. Kitchin, T. Bligaard, and H. Jonsson, J. Phys. Chem. B **108**, 17886 (2004).
[10] J. Greeley, I. Stephens, A. Bondarenko, T. Johansson, H. Hansen, T. Jaramillo, J. Rossmeisl, I. Chorkendorff, and J. Nørskov, Nat. Chem. **1**, 552 (2009).
[11] I. C. Man, H. Y. Su, F. Calle-Vallejo, H. A. Hansen, J. I. Martínez, N. G. Inoglu, J. Kitchin, T. F. Jaramillo, J. K. Nørskov, and J. Rossmeisl, ChemCatChem **3**, 1159 (2011).
[12] J. Rossmeisl, G. S. Karlberg, T. Jaramillo, and J. K. Norskov, Faraday Discuss. **140**, 337 (2009).
[13] P. Hohenberg and W. Kohn, Phys. Rev. **136**, B864 (1964).
[14] W. Kohn and L. Sham, Phys. Rev. **140**, A1133 (1965).
[15] J. Mortensen, L. Hansen, and K. Jacobsen, Phys. Rev. B: Condens. Matter **71**, 035109 (2005).
[16] J. Enkovaara, C. Rostgaard, J. Mortensen, J. Chen, M. Dułak, L. Ferrighi, J. Gavnholt, C. Glinsvad, V. Haikola, H. Hansen, H. Kristoffersen, M. Kuisma, A. Larsen, L. Lehtovaara, M. Ljungberg, O. Lopez-Acevedo, P. Moses, J. Ojanen, T. Olsen, V. Petzold, N. Romero, J. Stausholm-Møller, M. Strange, G. Tritsaris, M. Vanin, M. Walter, B. Hammer, H. Häkkinen, G. Madsen, R. Nieminen, J. Nørskov, M. Puska, T. Rantala, J. Schiøtz, K. Thygesen, and K. Jacobsen, J. Phys. Condens. Matter **22**, 253202 (2010).
[17] S. Bahn and K. Jacobsen, Comput. Sci. Eng. **4**, 56 (2002).
[18] J. Chen, J. Hummelshøj, K. Thygesen, J. Myrdal, J. Nørskov, and T. Vegge, Catal. Today **165**, 2 (2011).
[19] A. H. Larsen, M. Vanin, J. J. Mortensen, K. S. Thygesen, and K. W. Jacobsen, Phys. Rev. B: Condens. Matter **80**, 195112 (2009).
[20] J. M. Garcia-Lastra, J. Bass, and K. S. Thygesen, J. Chem. Phys. **135**, 121101 (2011).
[21] J. Simmons, J. Phys. D: Appl. Phys. **4**, 613 (1971).